

ARMY RESEARCH LABORATORY



**Dissipative Particle Dynamics at Isoenergetic Conditions
Using Shardlow-Like Splitting Algorithms**

by John K. Brennan and Martin Lísal

ARL-TR-6586

September 2013

NOTICES

Disclaimers

The findings in this report are not to be construed as an official Department of the Army position unless so designated by other authorized documents.

Citation of manufacturer's or trade names does not constitute an official endorsement or approval of the use thereof.

Destroy this report when it is no longer needed. Do not return it to the originator.

Army Research Laboratory

Aberdeen Proving Ground, MD 21005-5069

ARL-TR-6586

September 2013

Dissipative Particle Dynamics at Isoenergetic Conditions Using Shardlow-Like Splitting Algorithms

John K. Brennan

Weapons and Materials Research Directorate, ARL

Martin Lísal

Institute of Chemical Process Fundamentals of the ASCR

and

J. E. Purkinje University

REPORT DOCUMENTATION PAGE			Form Approved OMB No. 0704-0188		
Public reporting burden for this collection of information is estimated to average 1 hour per response, including the time for reviewing instructions, searching existing data sources, gathering and maintaining the data needed, and completing and reviewing the collection information. Send comments regarding this burden estimate or any other aspect of this collection of information, including suggestions for reducing the burden, to Department of Defense, Washington Headquarters Services, Directorate for Information Operations and Reports (0704-0188), 1215 Jefferson Davis Highway, Suite 1204, Arlington, VA 22202-4302. Respondents should be aware that notwithstanding any other provision of law, no person shall be subject to any penalty for failing to comply with a collection of information if it does not display a currently valid OMB control number. PLEASE DO NOT RETURN YOUR FORM TO THE ABOVE ADDRESS.					
1. REPORT DATE (DD-MM-YYYY) September 2013		2. REPORT TYPE Final		3. DATES COVERED (From - To) October 2011–January 2013	
4. TITLE AND SUBTITLE Dissipative Particle Dynamics at Isoenergetic Conditions Using Shardlow-Like Splitting Algorithms			5a. CONTRACT NUMBER		
			5b. GRANT NUMBER		
			5c. PROGRAM ELEMENT NUMBER		
6. AUTHOR(S) John K. Brennan and Martin Lísal*			5d. PROJECT NUMBER		
			5e. TASK NUMBER		
			5f. WORK UNIT NUMBER		
7. PERFORMING ORGANIZATION NAME(S) AND ADDRESS(ES) U.S. Army Research Laboratory ATTN: RDRL-WML-B Aberdeen Proving Ground, MD 21005-5069			8. PERFORMING ORGANIZATION REPORT NUMBER ARL-TR-6586		
9. SPONSORING/MONITORING AGENCY NAME(S) AND ADDRESS(ES)			10. SPONSOR/MONITOR'S ACRONYM(S)		
			11. SPONSOR/MONITOR'S REPORT NUMBER(S)		
12. DISTRIBUTION/AVAILABILITY STATEMENT Approved for public release; distribution is unlimited.					
13. SUPPLEMENTARY NOTES *E. Hála Laboratory of Thermodynamics, Institute of Chemical Process Fundamentals of the ASCR, v. v. i., Prague, Czech Republic and Department of Physics, Faculty of Science, J. E. Purkinje University, Ústí nad Labem, Czech Republic					
14. ABSTRACT A numerical integration scheme based upon the Shardlow-splitting algorithm (SSA) is presented for the Dissipative Particle Dynamics method at constant energy (DPD-E). The application of the SSA is particularly critical for the DPD-E variant because it allows more temporally practical simulations to be carried out. The DPD-E variant using the SSA is verified using both a standard DPD fluid model and a coarse-grain solid model. For both models, the DPD-E variant is further verified by instantaneously heating a slab of particles in the simulation cell and subsequently monitoring the evolution of the corresponding thermodynamic variables as the system approaches an equilibrated state while maintaining constant-energy conditions. The Fokker-Planck equation and derivation of the fluctuation-dissipation theorem are included.					
15. SUBJECT TERMS dissipative particle dynamics, mesoscale, simulation, Shardlow-splitting algorithm, constant-energy					
16. SECURITY CLASSIFICATION OF:			17. LIMITATION OF ABSTRACT	18. NUMBER OF PAGES	19a. NAME OF RESPONSIBLE PERSON John K. Brennan
a. REPORT Unclassified	b. ABSTRACT Unclassified	c. THIS PAGE Unclassified			UU

Contents

List of Figures	iv
List of Tables	iv
Acknowledgments	v
1. Introduction	1
2. Formulations of DPD at Fixed Total Energy Using Shardlow-Like Splitting	
Numerical Discretization	2
2.1 General Formulation of DPD	2
2.2 Constant-Energy DPD	3
2.2.1 Numerical Discretization	4
3. Computational Details	9
4. Results	10
4.1 Test Case 1: Equivalence of DPD Variants	10
4.1.1 DPD Fluid	10
4.1.2 Coarse-Grain Solid	13
4.2 Test Case 2: Heating Response in DPD-E Simulations	14
4.2.1 DPD Fluid	14
4.2.2 Coarse-Grain Solid	15
4.3 Conservation of Total System Energy	18
5. Conclusion	19
6. References	21
Appendix A. Fokker-Planck Equation and Fluctuation-Dissipation Theorem	23
Appendix B. Simulation Model Details	27
List of Symbols, Abbreviations, and Acronyms	29
Distribution List	30

List of Figures

Figure 1. Time evolution of the kinetic temperature T_{kin} , internal temperature T_{int} , and virial pressure P_{vir} for a DPD-E simulation of the pure DPD fluid at $\rho = 3$, where a slab of particles in the simulation box was instantaneously heated by $T_{heat} = 10$ at $t = 0$. Inset of figure displays early time behavior of T_{kin} , T_{int} , and P_{vir} .	15
Figure 2. (a) Time evolution of the kinetic temperature T_{kin} , internal temperature T_{int} , and virial pressure P_{vir} , along with (b) a few representative simulation snapshots for a DPD-E simulation of the coarse-grain solid at $\rho = 8260 \text{ kg/m}^3$, where a slab of particles in the simulation box was instantaneously heated by $T_{heat} = 3000 \text{ K}$ at $t = 0$.	16
Figure 3. The relative drift in E as a function of the integration time step Δt for DPD-E simulations with the SSA-VV	19

List of Tables

Table 1. The configurational energy per particle $\langle u \rangle$, the kinetic temperature $\langle T_{kin} \rangle$, the internal temperature $\langle T_{int} \rangle$, the virial pressure $\langle P_{vir} \rangle$, and the self-diffusion coefficient D determined from test case 1 simulations of the pure DPD fluid. $\langle \cdot \rangle$ denotes an ensemble average, where numbers in parentheses are uncertainties calculated from block averages.	12
Table 2. The configurational energy per particle $\langle u \rangle$, the kinetic temperature $\langle T_{kin} \rangle$, the internal temperature $\langle T_{int} \rangle$, the virial pressure $\langle P_{vir} \rangle$, and the self-diffusion coefficient D determined from test case 1 simulations of the equimolar binary DPD fluid. $\langle \cdot \rangle$ denotes an ensemble average, where numbers in parentheses are uncertainties calculated from block averages.	12
Table 3. The molar configurational energy $\langle u \rangle$, the kinetic temperature $\langle T_{kin} \rangle$, the internal temperature $\langle T_{int} \rangle$, and the virial pressure $\langle P_{vir} \rangle$ determined from test case 1 simulations of the coarse-grain solid model of nickel. $\langle \cdot \rangle$ denotes an ensemble average, where numbers in parentheses are uncertainties calculated from block averages.	13

Acknowledgments

Martin Lísal acknowledges that this research was sponsored by the U.S. Army Research Laboratory (ARL) and was accomplished under cooperative agreement number W911NF-10-2-0039. The views and conclusions contained in this document are those of the authors and should not be interpreted as representing the official policies, either expressed or implied, of ARL or the U.S. government. The U.S. government is authorized to reproduce and distribute reprints for government purposes notwithstanding any copyright notation herein. John K. Brennan acknowledges support in part by the Office of Naval Research and the Department of Defense High Performance Computing Modernization Program Software Application Institute for Multiscale Reactive Modeling of Insensitive Munitions.

INTENTIONALLY LEFT BLANK.

1. Introduction

An important extension of the original constant-temperature dissipative particle dynamics (DPD) method (1, 2) that imposes constant energy (DPD-E) conditions was developed by Bonet Avalos and Mackie (3) and later independently by Español (4). The DPD-E method includes an additional equation-of-motion that provides a dynamic depiction of the internal state of a coarse-grain particle. Consequently, particles are allowed to exchange both momentum and heat, thus satisfying total energy and momentum conservation.

Numerical integration of the equations of motion (EOMs) is a key consideration when applying the DPD method because the stochastic component requires special attention. Efficient and accurate integration schemes are required to maintain reasonable time step sizes, thus allowing for the simulation of mesoscale events. Moreover, the advent of conservative forces extending beyond purely repulsive models that contain attractive character further supports the need for effective integration schemes. However, the integration is a nontrivial task due to the pairwise coupling of particles through the random and dissipative forces (5). For example, the most widely used modified velocity-Verlet algorithm (6) works reasonably well for the constant-temperature DPD method, but for the DPD-E method it requires time-step values that are several orders of magnitude smaller than for constant-temperature DPD (7, 8).

Furthermore, self-consistent solutions are often necessary because the dissipative forces and the relative velocities of the particles are interdependent, where the considerable computational cost associated with this task has motivated the development of various integration schemes. Recent independent studies by Nikunen et al. (5) and Chaudhri and Lukes (9) assessed the quality and performance of several applicable integration schemes for constant-temperature DPD, where the Shardlow-splitting algorithm (SSA) (10) was identified as the best-performing approach. In recent work by our group (11, 12), a comprehensive description of numerical integration schemes based upon the SSA was presented for both the isothermal and isothermal, isobaric DPD methods. The original SSA formulated for systems of equal-mass particles was extended to systems of unequal-mass particles. Both a velocity-Verlet scheme and an implicit scheme were formulated for the integration of the fluctuation-dissipation contribution, where the velocity-Verlet scheme consistently performed better.

The SSA decomposes the EOM into differential equations that correspond to the deterministic dynamics and elementary stochastic differential equations that correspond to the stochastic dynamics. In the original SSA formulation, both types of differential equations are integrated via the velocity-Verlet algorithm (10), where the stochastic dynamics are additionally solved in an implicit manner that conserves linear momentum. Previously, the SSA had only been applied to the isothermal (10, 11) and isothermal, isobaric (12) DPD methods.

In this work, we formulate the SSA for the DPD-E method, where we verify the DPD-E variant using both the standard DPD fluid (pure and binary mixtures) (6) and a coarse-grain solid model (13). For both models, we further verify the DPD-E variant by instantaneously heating a slab of particles in the simulation cell. We monitor the evolution of the temperature and pressure as the system approaches an equilibrated state while maintaining constant energy. For completeness, the derivations of the Fokker-Planck equation (FPE) and the fluctuation-dissipation theorem (FDT) are included in appendix A.

2. Formulations of DPD at Fixed Total Energy Using Shardlow-Like Splitting Numerical Discretization

2.1 General Formulation of DPD

DPD particles are defined by a mass m_i , position \mathbf{r}_i , and momentum \mathbf{p}_i . The particles interact with each other via a pairwise force \mathbf{F}_{ij} that is written as the sum of a conservative force \mathbf{F}_{ij}^C , dissipative force \mathbf{F}_{ij}^D , and random force \mathbf{F}_{ij}^R :

$$\mathbf{F}_{ij} = \mathbf{F}_{ij}^C + \mathbf{F}_{ij}^D + \mathbf{F}_{ij}^R. \quad (1)$$

\mathbf{F}_{ij}^C is given as the negative derivative of a coarse-grain potential, u_{ij}^{CG} , expressed as

$$\mathbf{F}_{ij}^C = -\frac{du_{ij}^{CG}}{dr_{ij}} \frac{\mathbf{r}_{ij}}{r_{ij}}, \quad (2)$$

where $\mathbf{r}_{ij} = \mathbf{r}_i - \mathbf{r}_j$ is the separation vector between particle i and particle j , and $r_{ij} = |\mathbf{r}_{ij}|$. The remaining two forces, \mathbf{F}_{ij}^D and \mathbf{F}_{ij}^R , can be interpreted as a means to compensate for the degrees of freedom neglected by coarse graining. The conservative force is not specified by the DPD formulation and can be chosen to include any forces that are appropriate for a given application, including multibody interactions (e.g., [13–15]). \mathbf{F}_{ij}^D and \mathbf{F}_{ij}^R are defined as

$$\mathbf{F}_{ij}^D = -\gamma_{ij} \omega^D(r_{ij}) \left(\frac{\mathbf{r}_{ij}}{r_{ij}} \cdot \mathbf{v}_{ij} \right) \frac{\mathbf{r}_{ij}}{r_{ij}} \quad (3)$$

and

$$\mathbf{F}_{ij}^R = \sigma_{ij} \omega^R(r_{ij}) \mathcal{W}_{ij} \frac{\mathbf{r}_{ij}}{r_{ij}}, \quad (4)$$

where between particle i and j , γ_{ij} and σ_{ij} are the friction coefficient and noise amplitude, respectively, $\mathbf{v}_{ij} = \frac{\mathbf{p}_i}{m_i} - \frac{\mathbf{p}_j}{m_j}$ and W_{ij} are independent Wiener processes such that $W_{ij} = W_{ji}$. The weight functions $\omega^D(r)$ and $\omega^R(r)$ vanish for $r \geq r_c$, where r_c is the cutoff radius.

Note that \mathbf{F}_{ij}^C is completely independent of \mathbf{F}_{ij}^D and \mathbf{F}_{ij}^R , while \mathbf{F}_{ij}^D and \mathbf{F}_{ij}^R are not independent but rather are coupled through a fluctuation-dissipation relation. This coupling arises from the requirement that in the thermodynamic limit, the system samples the corresponding probability distribution. The necessary conditions can be derived using an FPE; these conditions are presented in appendix A for the DPD-E variant.

2.2 Constant-Energy DPD

The constant-energy DPD approach was developed by Bonet Avalos and Mackie (3), and shortly thereafter also by Español (4). To conserve energy in a DPD simulation, an additional variable is introduced that characterizes the internal state of the particles. An internal energy u_i (restricted to $u_i \geq 0$ always) is associated with each DPD particle, which accounts for the energy absorbed or released by the atomic internal degrees of freedom that have been coarse-grained into the DPD particle. The total energy of the system is conserved since the kinetic energy lost/gained by the dissipative and random interactions is absorbed/released by this particle internal energy. Taken along with u_i is an associated mesoscopic entropy $s_i = s(u_i)$, which is a monotonously increasing function of u_i , so that the internal temperature θ_i is defined as $\frac{1}{\theta_i} \equiv \frac{\partial s_i}{\partial u_i} > 0$ (16). A

mesoparticle equation of state relating θ_i and u_i is therefore required. It is convenient to write the variation of du_i as the sum of two contributions that correspond to the mechanical work done on the system du_i^{mech} and the heat conduction between particles du_i^{cond} , i.e., as $du_i = du_i^{mech} + du_i^{cond}$. The dynamics of the system is then governed by the following equations-of-motion (EOMs):

$$\begin{aligned}
d\mathbf{r}_i &= \frac{\mathbf{p}_i}{m_i} dt \\
d\mathbf{p}_i &= \sum_{j \neq i} \mathbf{F}_{ij}^C dt - \gamma_{ij} \omega^D \left(\frac{\mathbf{r}_{ij}}{r_{ij}} \cdot \mathbf{v}_{ij} \right) \frac{\mathbf{r}_{ij}}{r_{ij}} dt + \sigma_{ij} \omega^R \frac{\mathbf{r}_{ij}}{r_{ij}} dW_{ij} \\
du_i^{mech} &= \frac{1}{2} \sum_{j \neq i} \gamma_{ij} \omega^D \left(\frac{\mathbf{r}_{ij}}{r_{ij}} \cdot \mathbf{v}_{ij} \right)^2 dt - \frac{d\sigma_{ij}^2}{2} \left(\frac{1}{m_i} + \frac{1}{m_j} \right) (\omega^R)^2 dt \quad (i = 1, \dots, N), \\
&\quad - \sigma_{ij} \omega^R \left(\frac{\mathbf{r}_{ij}}{r_{ij}} \cdot \mathbf{v}_{ij} \right) dW_{ij} \\
du_i^{cond} &= \sum_{j \neq i} \kappa_{ij} \left(\frac{1}{\theta_i} - \frac{1}{\theta_j} \right) \omega^{Dq} dt + \alpha_{ij} \omega^{Rq} dW_{ij}^q
\end{aligned} \tag{5}$$

where $\omega^{Dq}(r)$ and $\omega^{Rq}(r)$ are weight functions vanishing for $r \geq r_c$, κ_{ij} and α_{ij} are the mesoscopic thermal conductivity and the noise amplitude between particle i and particle j , respectively, and $dW_{ij}^q = -dW_{ji}^q$ are the increments of the Wiener processes associated with thermal conduction. Equation 5 is a generalization of the modified DPD-E approach (16) for particles with unequal masses (17). In the last expression of equation 5, the first term on the right-hand side, which specifies the dissipative heat conduction, can alternatively be expressed in terms of the difference of particle temperatures (18).

Bonet Avalos and Mackie (3) demonstrated that thermodynamic consistency requires the following fluctuation-dissipation relations to be satisfied:

$$\begin{aligned}\sigma_{ij}^2 &= 2\gamma_{ij}k_B\Theta_{ij} \\ \omega^D(r) &= [\omega^R(r)]^2 \\ \alpha_{ij}^2 &= 2k_B\kappa_{ij} \\ \omega^{Dq}(r) &= [\omega^{Rq}(r)]^2\end{aligned}, \quad (6)$$

where the relevant temperature is $\Theta_{ij}^{-1} = \frac{1}{2}\left(\frac{1}{\theta_i} + \frac{1}{\theta_j}\right)$, and $\omega^{Dq}(r)$ and $\omega^{Rq}(r)$ can be chosen

similar to $\omega^D(r)$ and $\omega^R(r)$, respectively (11). (Bonet Avalos and Mackie [3] did not prove that the DPD-E EOMs sample the microcanonical ensemble, rather they proved that the relations in equation 6 are required for the EOMs to sample the canonical ensemble, where these relations are independent of T .) An outline of the derivation of these FDTs along with the FPE is given in appendix A. By design, these EOMs conserve total momentum \mathbf{P} and the total energy $E = U + K + \sum_i u_i$. Note that the random-force noise amplitude σ_{ij} depends on the particle

internal temperatures and not on the system temperature T as it does in the constant-temperature DPD method. (The system temperature in a DPD-E simulation is defined as $T = \frac{1}{3Nk_B} \sum_i \frac{\mathbf{p}_i \cdot \mathbf{p}_i}{m_i}$.)

2.2.1 Numerical Discretization

As part of the founding work, Mackie et al. (16) developed an explicit integration algorithm for the DPD-E approach. However, because of round-off error resulting from the loss of mechanical energy during integration of the work done by the dissipative and random forces, the algorithm requires a rather small Δt to satisfactorily conserve the total energy. This situation can be improved by extending the splitting strategy developed by Stoltz (17) to equation 5. Stoltz introduced a set of EOMs that closely resembles DPD-E except (1) they neglect thermal conduction, and (2) they do not project the dissipative and random forces along the separation vectors between the particles.

In the following paragraphs, we present an extension of Stoltz's splitting algorithm to DPD-E. As done previously (11, 12), we start by decomposing the EOMs given in equation 5 into deterministic differential equations and elementary stochastic differential equations (SDEs) based upon the conservative and fluctuation-dissipation contributions, respectively. The conservative terms are identical to the constant-temperature DPD formulation,

$$d\mathbf{r}_i = \frac{\mathbf{p}_i}{m_i} dt \quad (7a)$$

and

$$(i = 1, \dots, N)$$

$$d\mathbf{p}_i = \sum_{j \neq i} \mathbf{F}_{ij}^C dt, \quad (7b)$$

while the fluctuation-dissipation terms can be expressed as

$$d\mathbf{p}_i^{i-j} = -\gamma_{ij} \omega^D \left(\frac{\mathbf{r}_{ij}}{r_{ij}} \cdot \mathbf{v}_{ij} \right) \frac{\mathbf{r}_{ij}}{r_{ij}} dt + \sigma_{ij} \omega^R \frac{\mathbf{r}_{ij}}{r_{ij}} dW_{ij}, \quad (8a)$$

$$d\mathbf{p}_j^{i-j} = -d\mathbf{p}_i^{i-j}$$

$$du_i^{mech, i-j} = -\frac{1}{2} d \left(\frac{\mathbf{p}_i^{i-j} \cdot \mathbf{p}_i^{i-j}}{2m_i} + \frac{\mathbf{p}_j^{i-j} \cdot \mathbf{p}_j^{i-j}}{2m_j} \right) \quad \left(\text{for each } i < j \right), \quad (8b)$$

$$du_j^{mech, i-j} = du_i^{mech, i-j}$$

and

$$du_i^{cond, i-j} = \kappa_{ij} \left(\frac{1}{\theta_i} - \frac{1}{\theta_j} \right) \omega^{Dq} dt + \alpha_{ij} \omega^{Rq} dW_{ij}^q, \quad (8c)$$

$$du_j^{cond, i-j} = -du_i^{cond, i-j}$$

where the superscript $i-j$ indicates that the variation of momenta is considered for a pair of interacting particles i and j only, and $dW_{ij} = dW_{ji}$ are the increments of the Wiener processes.

Equation 8b directly follows from the introduction of the mechanical contribution to the internal energies (3, 4), where Mackie et al. (16) showed that the total energy of a pair of interacting particles i and j is conserved when

$$\frac{du_i^{mech, i-j}}{dt} \equiv \frac{du_j^{mech, i-j}}{dt} = -\frac{1}{2} \left(\frac{\mathbf{p}_i^{i-j}}{m_i} - \frac{\mathbf{p}_j^{i-j}}{m_j} \right) \cdot (\mathbf{F}_{ij}^D + \mathbf{F}_{ij}^R). \quad (9a)$$

Using equation 8a along with the definitions of \mathbf{F}_{ij}^D and \mathbf{F}_{ij}^R (equations 3 and 4, respectively), we can rewrite equation 9a as

$$\begin{aligned} \frac{d\mathbf{u}_i^{mech,i-j}}{dt} &= -\frac{1}{2} \left(\frac{\mathbf{p}_i^{i-j}}{m_i} \cdot \frac{d\mathbf{p}_i^{i-j}}{dt} + \frac{\mathbf{p}_j^{i-j}}{m_j} \cdot \frac{d\mathbf{p}_j^{i-j}}{dt} \right) \\ &= -\frac{1}{2} \frac{d}{dt} \left(\frac{\mathbf{p}_i^{i-j} \cdot \mathbf{p}_i^{i-j}}{2m_i} + \frac{\mathbf{p}_j^{i-j} \cdot \mathbf{p}_j^{i-j}}{2m_j} \right). \end{aligned} \quad (9b)$$

Equation 9b together with $\frac{d\mathbf{u}_i^{mech,i-j}}{dt} = \frac{d\mathbf{u}_j^{mech,i-j}}{dt}$ then leads to equation 8b. As done previously (11, 12), the stochastic flow map $\phi_{\Delta t}$ can be approximated from the first-order splitting algorithm given by

$$\phi_{\Delta t} \cong \phi_{\Delta t;1,2}^{diss} \circ \phi_{\Delta t;1,3}^{diss} \circ \dots \circ \phi_{\Delta t;i,j}^{diss} \circ \dots \circ \phi_{\Delta t;N-2,N}^{diss} \circ \phi_{\Delta t;N-1,N}^{diss} \circ \phi_{\Delta t}^C, \quad (10)$$

where \circ denotes a composition of operators. For each $\phi_{\Delta t;i,j}^{diss}$ term at fixed internal temperatures (θ_i and θ_j), momenta are updated through the Shardlow-splitting algorithm-velocity Verlet (SSA-VV) approach based upon the constant-temperature DPD formulation previously given (11).

$$\mathbf{p}_i \left(t + \frac{\Delta t}{2} \right) = \mathbf{p}_i(t) - \frac{\Delta t}{2} \gamma_{ij} \omega^D \left[\frac{\mathbf{r}_{ij}}{r_{ij}} \cdot \mathbf{v}_{ij}(t) \right] \frac{\mathbf{r}_{ij}}{r_{ij}} + \frac{\sqrt{\Delta t}}{2} \sigma_{ij} \omega^R \zeta_{ij} \frac{\mathbf{r}_{ij}}{r_{ij}}, \quad (11a)$$

$$\mathbf{p}_j \left(t + \frac{\Delta t}{2} \right) = \mathbf{p}_j(t) + \frac{\Delta t}{2} \gamma_{ij} \omega^D \left[\frac{\mathbf{r}_{ij}}{r_{ij}} \cdot \mathbf{v}_{ij}(t) \right] \frac{\mathbf{r}_{ij}}{r_{ij}} - \frac{\sqrt{\Delta t}}{2} \sigma_{ij} \omega^R \zeta_{ij} \frac{\mathbf{r}_{ij}}{r_{ij}}, \quad (11b)$$

$$\begin{aligned} \mathbf{p}_i(t + \Delta t) &= \mathbf{p}_i \left(t + \frac{\Delta t}{2} \right) - \frac{\Delta t}{2} \frac{\gamma_{ij} \omega^D}{1 + \frac{\mu_{ij}}{2} \gamma_{ij} \omega^D \Delta t} \left\{ \left[\frac{\mathbf{r}_{ij}}{r_{ij}} \cdot \mathbf{v}_{ij} \left(t + \frac{\Delta t}{2} \right) \right] \frac{\mathbf{r}_{ij}}{r_{ij}} + \sqrt{\Delta t} \frac{\mu_{ij}}{2} \sigma_{ij} \omega^R \zeta_{ij} \frac{\mathbf{r}_{ij}}{r_{ij}} \right\} \\ &\quad + \frac{\sqrt{\Delta t}}{2} \sigma_{ij} \omega^R \zeta_{ij} \frac{\mathbf{r}_{ij}}{r_{ij}} \end{aligned}, \quad (11c)$$

and

$$\begin{aligned} \mathbf{p}_j(t + \Delta t) &= \mathbf{p}_j \left(t + \frac{\Delta t}{2} \right) + \frac{\Delta t}{2} \frac{\gamma_{ij} \omega^D}{1 + \frac{\mu_{ij}}{2} \gamma_{ij} \omega^D \Delta t} \left\{ \left[\frac{\mathbf{r}_{ij}}{r_{ij}} \cdot \mathbf{v}_{ij} \left(t + \frac{\Delta t}{2} \right) \right] \frac{\mathbf{r}_{ij}}{r_{ij}} + \sqrt{\Delta t} \frac{\mu_{ij}}{2} \sigma_{ij} \omega^R \zeta_{ij} \frac{\mathbf{r}_{ij}}{r_{ij}} \right\} \\ &\quad - \frac{\sqrt{\Delta t}}{2} \sigma_{ij} \omega^R \zeta_{ij} \frac{\mathbf{r}_{ij}}{r_{ij}} \end{aligned}, \quad (11d)$$

where the superscript $i - j$ has been omitted for notational simplicity, and $\zeta_{ij} = \zeta_{ji}$ is a Gaussian random number with zero mean and unit variance that is chosen independently for each pair of interacting particles, and $\mu_{ij} = \frac{1}{m_i} + \frac{1}{m_j}$.

The conductive contribution to the internal energies is updated using an Euler algorithm. For the SSA-VV, this results in the following expressions:

$$\begin{aligned}
\mathbf{p}_i\left(t + \frac{\Delta t}{2}\right) &= \mathbf{p}_i(t) - \frac{\Delta t}{2} \gamma_{ij} \omega^D \left[\frac{\mathbf{r}_{ij}}{r_{ij}} \cdot \mathbf{v}_{ij}(t) \right] \frac{\mathbf{r}_{ij}}{r_{ij}} + \frac{\sqrt{\Delta t}}{2} \sigma_{ij} \omega^R \zeta_{ij} \frac{\mathbf{r}_{ij}}{r_{ij}} \\
\mathbf{p}_j\left(t + \frac{\Delta t}{2}\right) &= \mathbf{p}_j(t) + \frac{\Delta t}{2} \gamma_{ij} \omega^D \left[\frac{\mathbf{r}_{ij}}{r_{ij}} \cdot \mathbf{v}_{ij}(t) \right] \frac{\mathbf{r}_{ij}}{r_{ij}} - \frac{\sqrt{\Delta t}}{2} \sigma_{ij} \omega^R \zeta_{ij} \frac{\mathbf{r}_{ij}}{r_{ij}} \\
\mathbf{p}_i(t + \Delta t) &= \mathbf{p}_i\left(t + \frac{\Delta t}{2}\right) - \frac{\Delta t}{2} \frac{\gamma_{ij} \omega^D}{1 + \frac{\mu_{ij}}{2} \gamma_{ij} \omega^D \Delta t} \left\{ \left[\frac{\mathbf{r}_{ij}}{r_{ij}} \cdot \mathbf{v}_{ij}\left(t + \frac{\Delta t}{2}\right) \right] \frac{\mathbf{r}_{ij}}{r_{ij}} + \sqrt{\Delta t} \frac{\mu_{ij}}{2} \sigma_{ij} \omega^R \zeta_{ij} \frac{\mathbf{r}_{ij}}{r_{ij}} \right\} \\
&\quad + \frac{\sqrt{\Delta t}}{2} \sigma_{ij} \omega^R \zeta_{ij} \frac{\mathbf{r}_{ij}}{r_{ij}} \\
\mathbf{p}_j(t + \Delta t) &= \mathbf{p}_j\left(t + \frac{\Delta t}{2}\right) + \frac{\Delta t}{2} \frac{\gamma_{ij} \omega^D}{1 + \frac{\mu_{ij}}{2} \gamma_{ij} \omega^D \Delta t} \left\{ \left[\frac{\mathbf{r}_{ij}}{r_{ij}} \cdot \mathbf{v}_{ij}\left(t + \frac{\Delta t}{2}\right) \right] \frac{\mathbf{r}_{ij}}{r_{ij}} + \sqrt{\Delta t} \frac{\mu_{ij}}{2} \sigma_{ij} \omega^R \zeta_{ij} \frac{\mathbf{r}_{ij}}{r_{ij}} \right\} \\
&\quad - \frac{\sqrt{\Delta t}}{2} \sigma_{ij} \omega^R \zeta_{ij} \frac{\mathbf{r}_{ij}}{r_{ij}} \\
u_i^{cond}(t + \Delta t) &= u_i^{cond}(t) + \Delta t \kappa_{ij} \left(\frac{1}{\theta_i} - \frac{1}{\theta_j} \right) \omega^{Dq} + \sqrt{\Delta t} \alpha_{ij} \omega^{Rq} \zeta_{ij}^q \\
u_j^{cond}(t + \Delta t) &= u_j^{cond}(t) - \Delta t \kappa_{ij} \left(\frac{1}{\theta_i} - \frac{1}{\theta_j} \right) \omega^{Dq} - \sqrt{\Delta t} \alpha_{ij} \omega^{Rq} \zeta_{ij}^q
\end{aligned} \tag{12a}$$

In equation 12a, $\zeta_{ij}^q = -\zeta_{ji}^q$ is a Gaussian random number with zero mean and unit variance, chosen independently for each pair of interacting particles. Next, the mechanical contribution to the internal energies is updated using

$$\begin{aligned}
u_i^{mech}(t + \Delta t) &= u_i^{mech}(t) - \frac{1}{2} \left[\frac{\mathbf{p}_i(t + \Delta t) \cdot \mathbf{p}_i(t + \Delta t)}{2m_i} + \frac{\mathbf{p}_j(t + \Delta t) \cdot \mathbf{p}_j(t + \Delta t)}{2m_j} \right. \\
&\quad \left. - \frac{\mathbf{p}_i(t) \cdot \mathbf{p}_i(t)}{2m_i} - \frac{\mathbf{p}_j(t) \cdot \mathbf{p}_j(t)}{2m_j} \right] \\
u_j^{mech}(t + \Delta t) &= u_j^{mech}(t) - \frac{1}{2} \left[\frac{\mathbf{p}_i(t + \Delta t) \cdot \mathbf{p}_i(t + \Delta t)}{2m_i} + \frac{\mathbf{p}_j(t + \Delta t) \cdot \mathbf{p}_j(t + \Delta t)}{2m_j} \right. \\
&\quad \left. - \frac{\mathbf{p}_i(t) \cdot \mathbf{p}_i(t)}{2m_i} - \frac{\mathbf{p}_j(t) \cdot \mathbf{p}_j(t)}{2m_j} \right].
\end{aligned} \tag{12b}$$

In equations 12a and 12b, the superscript $i - j$ is again omitted for notational simplicity. The total system energy is exactly conserved via equation 12b. Finally, $\phi_{\Delta t}^C$ can be approximated by the velocity-Verlet algorithm previously given (11).

$$\begin{aligned}
\mathbf{p}_i\left(t + \frac{\Delta t}{2}\right) &= \mathbf{p}_i(t) + \frac{\Delta t}{2} \mathbf{F}_i^C(t) \\
\mathbf{r}_i(t + \Delta t) &= \mathbf{r}_i(t) + \Delta t \frac{\mathbf{p}_i\left(t + \frac{\Delta t}{2}\right)}{m_i} \quad (i = 1, \dots, N) \\
&\quad \text{evaluate } \{\mathbf{F}_i^C(t + \Delta t)\}_{i=1}^N \\
\mathbf{p}_i(t + \Delta t) &= \mathbf{p}_i\left(t + \frac{\Delta t}{2}\right) + \frac{\Delta t}{2} \mathbf{F}_i^C(t + \Delta t) \quad (i = 1, \dots, N)
\end{aligned} \tag{13}$$

The following outline summarizes a practical implementation of the SSA-VV for the DPD-E variant.

1. *Stochastic Integration* for all $i - j$ pairs of particles

- (i) $\mathbf{p}'_i \leftarrow \mathbf{p}_i, \mathbf{p}'_j \leftarrow \mathbf{p}_j$
- (ii) $\mathbf{p}_i \leftarrow \mathbf{p}_i - \frac{\Delta t}{2} \gamma_{ij} \omega^D \left(\frac{\mathbf{r}_{ij}}{r_{ij}} \cdot \mathbf{v}_{ij} \right) \frac{\mathbf{r}_{ij}}{r_{ij}} + \sigma_{ij} \omega^R \zeta_{ij} \frac{\mathbf{r}_{ij}}{r_{ij}} \frac{\sqrt{\Delta t}}{2}$
- (iii) $\mathbf{p}_j \leftarrow \mathbf{p}_j + \frac{\Delta t}{2} \gamma_{ij} \omega^D \left(\frac{\mathbf{r}_{ij}}{r_{ij}} \cdot \mathbf{v}_{ij} \right) \frac{\mathbf{r}_{ij}}{r_{ij}} - \sigma_{ij} \omega^R \zeta_{ij} \frac{\mathbf{r}_{ij}}{r_{ij}} \frac{\sqrt{\Delta t}}{2}$
- (iv) $\mathbf{v}_{ij} \leftarrow \frac{\mathbf{p}_i - \mathbf{p}_j}{m_i - m_j}$
- (v) $\mathbf{p}_i \leftarrow \mathbf{p}_i - \frac{\Delta t}{2} \frac{\gamma_{ij} \omega^D}{1 + \frac{\mu_{ij}}{2} \gamma_{ij} \omega^D \Delta t} \left[\left(\frac{\mathbf{r}_{ij}}{r_{ij}} \cdot \mathbf{v}_{ij} \right) \frac{\mathbf{r}_{ij}}{r_{ij}} + \frac{\mu_{ij}}{2} \sigma_{ij} \omega^R \zeta_{ij} \frac{\mathbf{r}_{ij}}{r_{ij}} \sqrt{\Delta t} \right] + \sigma_{ij} \omega^R \zeta_{ij} \frac{\mathbf{r}_{ij}}{r_{ij}} \frac{\sqrt{\Delta t}}{2}$

$$(vi) \quad \mathbf{p}_j \leftarrow \mathbf{p}_j + \frac{\Delta t}{2} \frac{\gamma_{ij} \omega^D}{1 + \frac{\mu_{ij}}{2} \gamma_{ij} \omega^D \Delta t} \left[\left(\frac{\mathbf{r}_{ij}}{r_{ij}} \cdot \mathbf{v}_{ij} \right) \frac{\mathbf{r}_{ij}}{r_{ij}} + \frac{\mu_{ij}}{2} \sigma_{ij} \omega^R \zeta_{ij} \frac{\mathbf{r}_{ij}}{r_{ij}} \sqrt{\Delta t} \right] - \sigma_{ij} \omega^R \zeta_{ij} \frac{\mathbf{r}_{ij}}{r_{ij}} \frac{\sqrt{\Delta t}}{2}$$

$$(vii) \quad u_i^{cond} \leftarrow u_i^{cond} + \kappa_{ij} \left(\frac{1}{\theta_i} - \frac{1}{\theta_j} \right) \omega^{Dq} \Delta t + \alpha_{ij} \omega^{Rq} \zeta_{ij}^q \sqrt{\Delta t}$$

$$(viii) \quad u_j^{cond} \leftarrow u_j^{cond} - \kappa_{ij} \left(\frac{1}{\theta_i} - \frac{1}{\theta_j} \right) \omega^{Dq} \Delta t - \alpha_{ij} \omega^{Rq} \zeta_{ij}^q \sqrt{\Delta t}$$

$$(ix) \quad u_i^{mech} \leftarrow u_i^{mech} - \frac{1}{2} \left[\frac{\mathbf{p}_i \cdot \mathbf{p}_i}{2m_i} + \frac{\mathbf{p}_j \cdot \mathbf{p}_j}{2m_j} - \frac{\mathbf{p}'_i \cdot \mathbf{p}'_i}{2m_i} - \frac{\mathbf{p}'_j \cdot \mathbf{p}'_j}{2m_j} \right]$$

$$(x) \quad u_j^{mech} \leftarrow u_j^{mech} - \frac{1}{2} \left[\frac{\mathbf{p}_i \cdot \mathbf{p}_i}{2m_i} + \frac{\mathbf{p}_j \cdot \mathbf{p}_j}{2m_j} - \frac{\mathbf{p}'_i \cdot \mathbf{p}'_i}{2m_i} - \frac{\mathbf{p}'_j \cdot \mathbf{p}'_j}{2m_j} \right]$$

2. *Deterministic Integration #1* for $i = 1, \dots, N$

$$(i) \quad \mathbf{p}_i \leftarrow \mathbf{p}_i + \frac{\Delta t}{2} \mathbf{F}_i^C$$

$$(ii) \quad \mathbf{r}_i \leftarrow \mathbf{r}_i + \Delta t \frac{\mathbf{p}_i}{m_i}$$

3. *Conservative Force Calculation*: $\{\mathbf{F}_i^C\}_{i=1}^N$

4. *Deterministic Integration #2* for $i = 1, \dots, N$

$$\mathbf{p}_i \leftarrow \mathbf{p}_i + \frac{\Delta t}{2} \mathbf{F}_i^C$$

3. Computational Details

The SSA-VV for the DPD-E variant was tested using both the standard DPD fluid (6) and a coarse-grain solid model (13), where complete details of the conservative forces for these models are given in appendix B. Both a pure component case and an equimolar binary mixture were tested for the DPD fluid model. System sizes for the DPD fluids and coarse-grain solid were, respectively, $N = 10125$ and 13500 . For these simulations, the following reduced units were used: r_c and r_0 are the unit of length for the DPD fluid and coarse-grain solid, respectively; the mass of a DPD particle is the unit of mass; and the unit of energy is $k_B T_{mi}$, where T_{mi} is the initial system temperature. Using these reduced units, we set the maximum repulsion between particles i and j as $a_{ij} = 25$ for the pure DPD fluid, and as $a_{ij} = 25$ and 28 for the like and unlike $i - j$ interactions, respectively, for the binary DPD fluid. Further, for all cases, we set the

noise amplitude $\sigma_{ij} = 3$. Next, we assume that the internal degrees of freedom are purely harmonic and express the coarse-grain particle equation of state as $u_i = C_{V,i}\theta_i$, with heat capacity $C_{V,i}/k_B \equiv C_V/k_B = 60$ and 48 for the pure DPD fluid and coarse-grain solid, respectively. Note that these values correspond to coarse-graining approximately 20 atoms and 16 atoms into a DPD particle, respectively (19). For the binary DPD fluid, we set $m_2 = 10m_1$ and $C_{V,2} = 10C_{V,1}$, where $C_{V,1}/k_B = 60$. Finally, following Ripoll et al. (20), the mesoscopic thermal conductivity κ_{ij} is chosen as

$$\kappa_{ij} = \kappa_0 \frac{C_V^2}{4k_B} (\theta_i + \theta_j)^2, \quad (14)$$

where κ_0 is the parameter controlling the thermal conductivity of the DPD particles, which are chosen as $\kappa_0 = 2.80 \cdot 10^{-4}$ for the pure DPD fluid and $\kappa_0 = 1.52 \cdot 10^{-4}$ for the coarse-grain solid. For the binary fluid, we set $\kappa_{0,11} = 2.80 \cdot 10^{-4}$, $\kappa_{0,22} = 2.80 \cdot 10^{-6}$, and $\kappa_{0,12} = \sqrt{\kappa_{0,11}\kappa_{0,22}}$. When $\theta_i = \theta_j = 1$, these particular values of κ_0 and C_V give $\kappa_{ij} = 1$.

4. Results

This section is organized as follows. The validity of the SSA integration algorithm for the DPD-E variant is verified by considering equilibrium and nonequilibrium scenarios, where results are given in subsections 4.1 and 4.2, respectively. Finally, we briefly review the energy drift associated with finite integration methods and propose a simple strategy to minimize these drifts in DPD-E simulations.

4.1 Test Case 1: Equivalence of DPD Variants

As a first test of the SSA-VV formulation for the DPD-E variant, we verify that it converges to the same equilibrium properties when at the same thermodynamic conditions as a constant-temperature DPD simulation.

4.1.1 DPD Fluid

The benchmark systems for both the pure and binary DPD fluid cases are taken from a constant-temperature DPD simulation performed at $\rho = 3$ and $T = 1$, and run for $t_{run} = 3000$ and $\Delta t = 0.03$. The following quantities were evaluated and are listed in tables 1 (pure fluid) and 2 (equimolar binary fluid): virial pressure $\langle P_{vir} \rangle$, configurational energy per particle $\langle u \rangle$, kinetic temperature $\langle T_{kin} \rangle$, and self-diffusion coefficients D using the Einstein relation (21).

To validate the constant-energy SSA-VV formulation, DPD-E simulations were performed at conditions taken from the constant-temperature DPD simulation, i.e., $V = L^3 = 3375$ (L is the box length). The final configuration of the constant-temperature DPD simulation is used to determine the imposed values of E , thus it is also used as the starting configuration for the DPD-E simulation. For both the pure and equimolar binary fluid cases, the values of u_i were initialized by setting $u_i = C_{v,i} T_{ini}$, where $T_{ini} = T = 1$, and were carried out for $t_{run} = 3000$ and $\Delta t = 0.01$. Analogous to microcanonical MD simulations, the use of a smaller Δt , with respect to constant-temperature DPD simulations, is required for proper conservation of E . Using $\Delta t = 0.01$, we observed a relative drift in E no greater than $1 \cdot 10^{-4}$. (For the DPD fluid simulations, reported relative drifts refer to an average of relative drifts over time periods of 1000.)

Comparing the DPD-E results with the constant-temperature DPD results in tables 1 and 2, we find excellent overall agreement. For the DPD-E simulations, the internal temperature,

$$\langle T_{int} \rangle = \left\langle \frac{1}{N} \sum_{i=1}^N \frac{1}{\theta_i} \right\rangle^{-1}$$

was also evaluated, where the values of $\langle T_{kin} \rangle$ and $\langle T_{int} \rangle$ agree within

statistical uncertainties. (Since θ_i is defined as a ratio of s_i and u_i , $\langle T_{int} \rangle$ is estimated through a harmonic average rather than an arithmetic average [16, 17].) For the pure DPD fluid, these values are approximately 1.5% lower than $T_{ini} = 1$; however, this discrepancy is due to the fundamental differences between the constant-temperature DPD and DPD-E methods.

Effectively, the two systems are different since the imposed temperature for the constant-temperature DPD system should be equivalent to $\langle T_{kin} \rangle$, while in the DPD-E system the total energy initially given to the system is dynamically partitioned among the kinetic and internal energies, yielding a variation in the equilibrium temperature with respect to T_{ini} (16). This difference is of $O(k_B / C_v)$ as compared with unity, while an additional contribution of the same order arises from the ‘‘extra degree-of-freedom’’ due to the fluctuations in u_i , since the relevant

macroscopic temperature is related to $\left(\frac{1}{\theta_i} \right)^{-1}$. Hence, for a pure DPD fluid up to first order in

k_B / C_v , $\langle T_{kin} \rangle = \langle T_{int} \rangle \cong T_{ini} (1 - k_B / C_v) \cong 0.983$ (16), in agreement with the simulated values of 0.985 ± 0.003 . For the equimolar binary fluid, the simulated values are also in agreement with the estimate $\langle T_{kin} \rangle = \langle T_{int} \rangle \cong 0.994$. The estimated value is closer to $T_{ini} = 1$ because of the larger value of $C_{v,2}$ that reduces the (k_B / C_v) contribution. Also note that because of these lower values of $\langle T_{kin} \rangle$ and $\langle T_{int} \rangle$, the values of $\langle P_{vir} \rangle$ in tables 1 and 2 slightly differ from $\langle P_{vir} \rangle$ for constant-temperature DPD.

Table 1. The configurational energy per particle $\langle u \rangle$, the kinetic temperature $\langle T_{kin} \rangle$, the internal temperature $\langle T_{int} \rangle$, the virial pressure $\langle P_{vir} \rangle$, and the self-diffusion coefficient D determined from test case 1 simulations of the pure DPD fluid. $\langle \cdot \rangle$ denotes an ensemble average, where numbers in parentheses are uncertainties calculated from block averages.

Variant	$\langle u \rangle$	$\langle T_{kin} \rangle$	$\langle T_{int} \rangle$	$\langle P_{vir} \rangle$	D
DPD $\rho = 3$	4.56(1)	1.005(8)	—	23.65(8)	0.295(13)
DPD-E $\rho = 3$	4.54(1)	0.985(8)	0.985(3)	23.61(11)	0.293(6)

Table 2. The configurational energy per particle $\langle u \rangle$, the kinetic temperature $\langle T_{kin} \rangle$, the internal temperature $\langle T_{int} \rangle$, the virial pressure $\langle P_{vir} \rangle$, and the self-diffusion coefficient D determined from test case 1 simulations of the equimolar binary DPD fluid. $\langle \cdot \rangle$ denotes an ensemble average, where numbers in parentheses are uncertainties calculated from block averages.

Variant	$\langle u \rangle$	$\langle T_{kin} \rangle$	$\langle T_{int} \rangle$	$\langle P_{vir} \rangle$	D_1	D_2
DPD $\rho = 3$	4.76(1)	1.005(8)	—	24.79(13)	0.177(13)	0.165(13)
DPD-E $\rho = 3$	4.75(1)	0.993(8)	0.994(3)	24.77(21)	0.174(9)	0.161(10)

Reproducing equilibrium averages is necessary but not sufficient proof that the integration scheme is behaving properly. Hence, as a further demonstration of the quality of the SSA-VV and the proper choice of Δt , for the pure DPD fluid, we calculated probability distributions for p_i , u_i , and V for constant-temperature DPD with $\Delta t = 0.03$ and for DPD-E with $\Delta t = 0.01$. We compared the probability distribution for p_i with the corresponding Maxwell-Boltzmann distribution (21), while the probability distributions for u_i and V were compared with those obtained with a very small $\Delta t = 0.001$, which is more than an order of magnitude smaller than typical values of Δt used and thus is approximated as the “exact” result. For a special case of DPD-E in the absence of conservative forces, an analytical form of the probability distribution for u_i was derived by Mackie et al. (16) under constant-temperature conditions. Probability distributions from constant-temperature DPD and DPD-E (not shown here) are in extremely good agreement.

4.1.2 Coarse-Grain Solid

We now perform a validation study analogous to the DPD fluids study for a coarse-grain solid model, where we consider a recently developed nickel model that reasonably reproduces several measured properties, including the melting temperature (13). For a benchmark system, a constant-temperature DPD simulation is performed at $\rho = 8260 \text{ kg/m}^3$ and $T = 1300 \text{ K}$ for $t_{run} = 1 \text{ ns}$ and $\Delta t = 5 \text{ fs}$, where results are listed in table 3. (Since the coarse-grain solid model has been parameterized to an actual material, results are reported in real units as opposed to reduced units for the DPD fluid.) At this state point, the atomistic Sutton-Chen (SC) model of nickel predicts a pressure of approximately 0 bar (13), while $\langle P_{vir} \rangle$ for the coarse-grain solid model is larger than 0 bar.

Analogous to the DPD fluid study, DPD-E simulations were performed at conditions determined from the constant-temperature DPD simulation. The value of E imposed in the DPD-E simulation was determined from the final configuration of the constant-temperature DPD simulation, which is used as the starting configuration. The value of u_i was initialized by setting $u_i = C_V T_{ini}$, where $T_{ini} = T = 1300 \text{ K}$. The simulation was run for $t_{run} = 1 \text{ ns}$ and $\Delta t = 5 \text{ fs}$, where a relative drift in E under $2 \cdot 10^{-4}$ was observed. (For the coarse-grain solid simulations, reported relative drifts refer to an average of relative drifts over time periods of 1 ns.) Comparing the DPD-E results with the constant-temperature DPD results in table 3, excellent overall agreement is found. For DPD-E, the values of $\langle T_{kin} \rangle$ and $\langle T_{int} \rangle$ are equal within statistical uncertainties. These values are approximately 2% lower than $T_{ini} = 1300 \text{ K}$ but agree within statistical uncertainties when the extra degree of freedom due to the fluctuations in u_i is considered, i.e., $\langle T_{kin} \rangle = \langle T_{int} \rangle \cong T_{ini} (1 - k_B / C_v) \cong 1273 \text{ K}$ (16). Furthermore, because of these lower values of $\langle T_{kin} \rangle$ and $\langle T_{int} \rangle$, the value of $\langle P_{vir} \rangle$ for DPD-E in table 3 differs accordingly from $\langle P_{vir} \rangle$ for constant-temperature DPD.

Table 3. The molar configurational energy $\langle u \rangle$, the kinetic temperature $\langle T_{kin} \rangle$, the internal temperature $\langle T_{int} \rangle$, and the virial pressure $\langle P_{vir} \rangle$ determined from test case 1 simulations of the coarse-grain solid model of nickel. $\langle \cdot \rangle$ denotes an ensemble average, where numbers in parentheses are uncertainties calculated from block averages.

Variant	$\langle u \rangle$ (kJ/mol)	$\langle T_{kin} \rangle$ (K)	$\langle T_{int} \rangle$ (K)	$\langle P_{vir} \rangle$ (bar)
DPD $\rho = 8260 \text{ kg/m}^3$	-508.44(11)	1300.1(91)	—	5.91(94)
DPD-E $\rho = 8260 \text{ kg/m}^3$	-508.71(11)	1274.8(88)	1274.5(5)	-150.49(98)

4.2 Test Case 2: Heating Response in DPD-E Simulations

As a second test case to verify the SSA-VV formulation for the DPD-E variant, a nonequilibrium scenario was considered for both the DPD fluids and the coarse-grain solid model. Starting from a final configuration of a constant-temperature DPD simulation, we instantaneously heated a slab of DPD particles in the middle of the simulation box and studied the system response at constant- (V, E) conditions, i.e., by DPD-E simulations.

4.2.1 DPD Fluid

Analogous to test case 1, the final configuration from the constant-temperature DPD simulation (at $T = 1$ and $\rho = 3$) was used as the starting configuration. For this configuration, a $0.5L$ wide slab of particles in the middle of the simulation box was heated by assigning velocities from a Maxwell-Boltzmann distribution corresponding to T_{heat} and by setting $u_i = C_{V,i} T_{heat}$. The remaining (nonheated) particles were assigned $u_i = C_{V,i} T_{ini}$, where $T_{ini} = T = 1$. As a test of the DPD-E variant, a simulation was performed using $T_{heat} = 10$, for $t_{run} = 5000$ and $\Delta t = 0.005$ for the pure and equimolar binary DPD fluids. Results for the time evolution of T_{kin} , T_{int} and P_{vir} for the pure DPD fluid are displayed in Fig. 1, where a relative drift of $2 \cdot 10^{-5}$ in E was observed. From figure 1, it is evident that T_{kin} and T_{int} quickly equalized, after which, T_{kin} , T_{int} and P_{vir} increased with t until the system reached equilibrium at $t > 150$. The inset of figure 1 displays the early time behavior of T_{kin} , T_{int} , and P_{vir} . Within $t \cong 10$, T_{kin} and P_{vir} sharply decreased from their initial values, followed by increasing values as the system moved toward an equilibrium state. The initial dramatic decreases in T_{kin} and P_{vir} are associated with the relaxation of the interfaces between “cold” and “hot” regions in the simulation box, which were artificially created by the instantaneous heating at $t = 0$. We found analogous results for the equimolar binary DPD fluid (not shown).

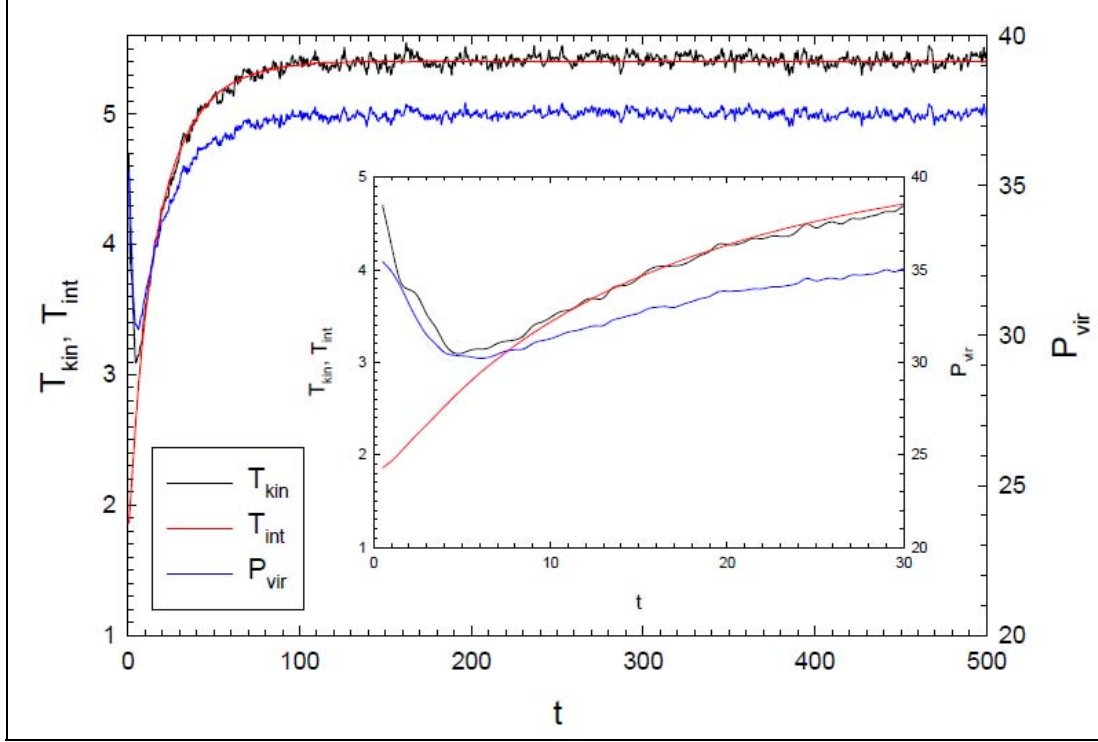


Figure 1. Time evolution of the kinetic temperature T_{kin} , internal temperature T_{int} , and virial pressure P_{vir} for a DPD-E simulation of the pure DPD fluid at $\rho = 3$, where a slab of particles in the simulation box was instantaneously heated by $T_{heat} = 10$ at $t = 0$. Inset of figure displays early time behavior of T_{kin} , T_{int} , and P_{vir} .

4.2.2 Coarse-Grain Solid

A validation study analogous to the DPD fluid study was carried out for the coarse-grain solid model of nickel. The final configuration from the constant-temperature DPD simulation (at $T = 1300$ K and $\rho = 8260$ kg/m³) was used as the starting configuration. From this starting configuration, a $0.5L$ wide slab of particles in the middle of the simulation box was heated by assigning velocities from a Maxwell-Boltzmann distribution corresponding to T_{heat} and by setting $u_i = C_V T_{heat}$. The remaining (nonheated) particles were assigned $u_i = C_V T_{ini}$, where $T_{ini} = T = 1300$ K. As a test of the DPD-E variant, simulations were performed at $\rho = 8260$ kg/m³, using $T_{heat} = 3000$ K for $t_{run} = 1$ ns and $\Delta t = 5$ fs. We observed relative drifts of $2 \cdot 10^{-4}$ in E . At low and moderate pressures, the coarse-grain solid model melts between 1800 and 1850 K (13). As a result, at the end of the DPD-E run, the particle configuration corresponds to a liquid state. Figure 2 shows the time evolution of T_{kin} , T_{int} , and P_{vir} (together with a few representative simulation snapshots) for the DPD-E simulation. Complete melting is evidenced by reaching a plateau in the time evolution of P_{vir} for the DPD-E simulation, where complete melting occurs at ~ 0.7 ns.

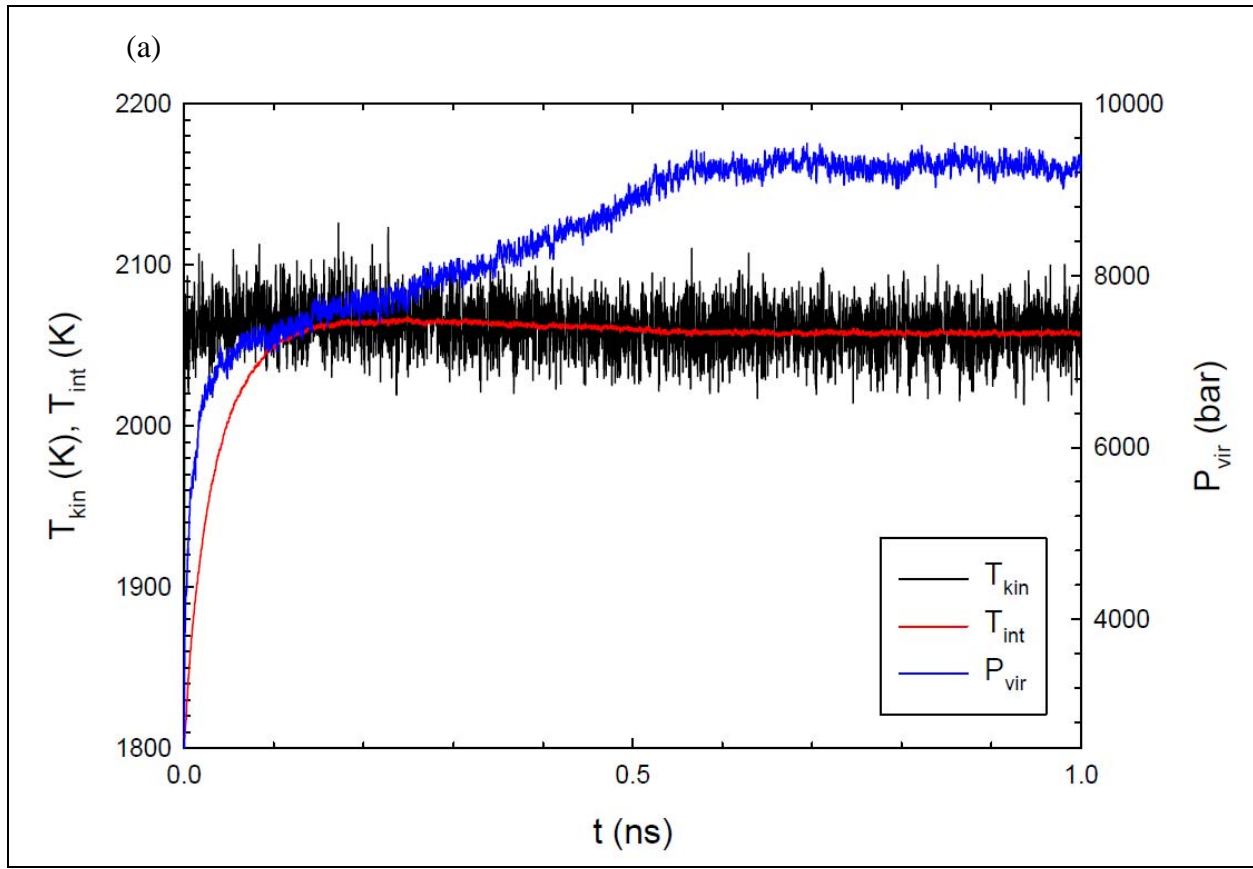


Figure 2. (a) Time evolution of the kinetic temperature T_{kin} , internal temperature T_{int} , and virial pressure P_{vir} , along with (b) a few representative simulation snapshots for a DPD-E simulation of the coarse-grain solid at $\rho = 8260 \text{ kg/m}^3$, where a slab of particles in the simulation box was instantaneously heated by $T_{heat} = 3000 \text{ K}$ at $t = 0$.

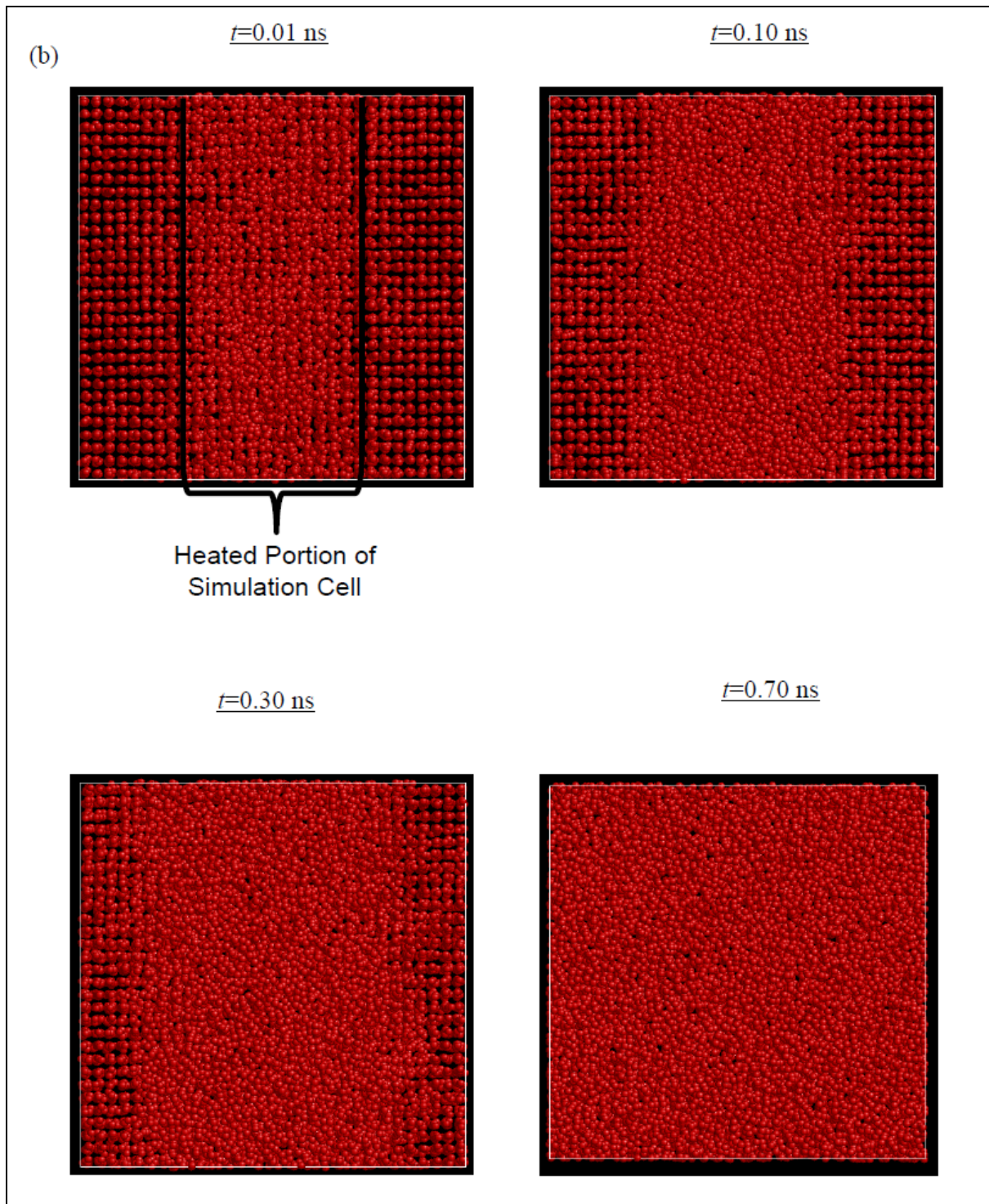


Figure 2. (a) Time evolution of the kinetic temperature T_{kin} , internal temperature T_{int} , and virial pressure P_{vir} , along with (b) a few representative simulation snapshots for a DPD-E simulation of the coarse-grain solid at $\rho = 8260$ kg/m³, where a slab of particles in the simulation box was instantaneously heated by $T_{heat} = 3000$ K at $t = 0$ (continued).

4.3 Conservation of Total System Energy

In practice, the SSA involves integrating the fluctuation-dissipation contribution and the conservative contribution in separate, independent steps. First, by implementing equation 18b rather than numerical discretization of equation 5, the integration of the fluctuation-dissipation contribution exactly conserves the total energy E at each time step. Second, analogous to an application of the velocity-Verlet algorithm in microcanonical molecular dynamics (MD), the integration of the conservative contribution does not conserve E at each time step. (DPD-E reduces to microcanonical MD in the limit of vanishing dissipative and random forces and heat transfers.) Rather, the velocity-Verlet algorithm preserves E only up to terms of order Δt^2 , conserving a pseudo-Hamiltonian that differs from the true Hamiltonian by this difference of order Δt^2 (22–25). Although the velocity-Verlet algorithm is area-preserving, it is not exactly symplectic. (An algorithm is area-preserving if $\text{drdp} = \text{const.}$, where $\mathbf{r} \equiv \{\mathbf{r}_i\}_{i=1}^N$ and $\mathbf{p} \equiv \{\mathbf{p}_i\}_{i=1}^N$.) The velocity-Verlet algorithm in microcanonical MD thus produces a long-term energy drift. Nonetheless, because of its area-preserving property, the velocity-Verlet algorithm is more stable at long times than non-area-preserving schemes, since system trajectories in phase space that are initially close will remain close during the microcanonical simulation (22).

For values of Δt comparable to those used in constant-temperature DPD simulations, we observed a small long-term drift in E for the DPD-E simulations. For example, for the values of Δt used for the DPD-E simulations in this work ($\Delta t = 0.01$ for the DPD fluids and $\Delta t = 5$ fs for the coarse-grain solid), the small relative drift produced in E was typically of order 10^{-4} . When Δt was decreased by an order of magnitude, the relative drift in E dropped to order 10^{-7} . A typical example of the dependence of the relative drift in E on Δt for the DPD fluid is shown in figure 3. The values of other properties (not shown here), such as the kinetic and internal temperatures, configurational energy, and virial pressure, change with Δt by less than 0.5%. This behavior is comparable with microcanonical MD simulations when the velocity-Verlet algorithm is used to integrate the EOM (21). Since the integration of the fluctuation-dissipation contribution exactly conserves the energy (up to machine precision), the drift is caused by the velocity-Verlet algorithm during the integration of the deterministic contribution in the DPD-E EOM. Similar to microcanonical MD, a long-term drift in E is thus inevitable in the SSA for DPD-E. Notably, a recent application of the standard velocity-Verlet algorithm to DPD-E for the DPD fluid model by Abu-Nada (7, 8) required $\Delta t = 0.00002$ to 0.00005 , i.e., values of Δt that are several orders of magnitude smaller than for constant-temperature DPD to minimize a drift in E .

To enforce constant energy beyond this small drift, one can apply the following numerical procedure. After each time step, the difference between the current E and the inputted E is calculated. This difference is then divided by the number of particles and equally subtracted from each u_i . This is a useful strategy provided that the drift in E has a mechanical origin, which

implies that the energy drift scales as $k_B T$. Thus, the extra energy per particle subtracted in this procedure is very small compared to the magnitude of u_i , which scales as $C_v T$. In this work, the variation of the system temperature due to this drift was negligible and the dynamics unaffected. This strategy was applied to all test cases for DPD-E, where we observed no variation in the results.

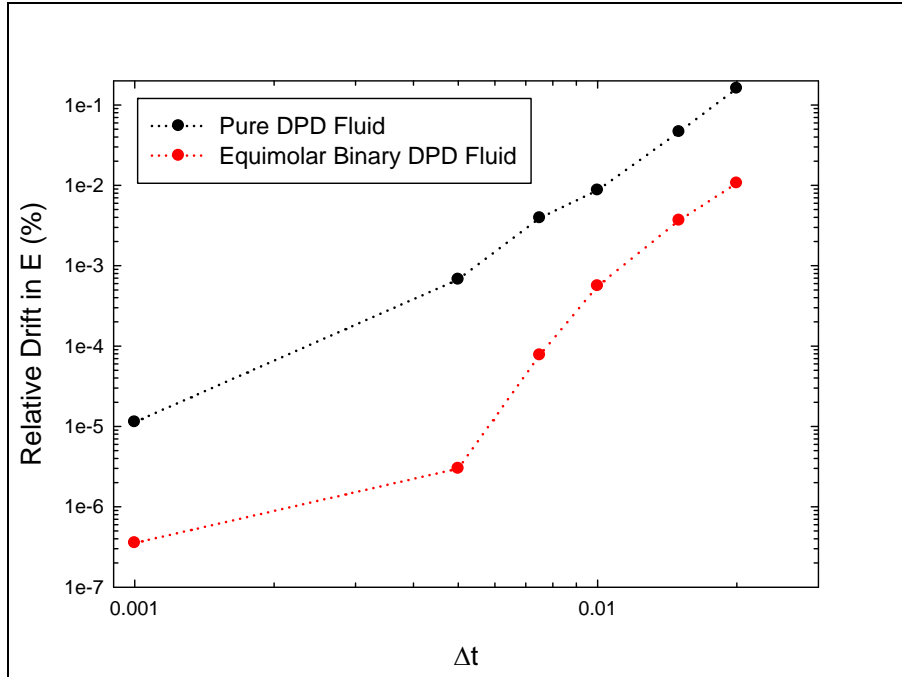


Figure 3. The relative drift in E as a function of the integration time step Δt for DPD-E simulations with the SSA-VV.

5. Conclusion

We presented a comprehensive description of a numerical integration scheme based upon the SSA for the DPD-E approach, where it was readily extendable and found to be a stable and accurate integration scheme. The DPD-E variant was verified using both a standard DPD fluid model and a coarse-grain solid model, where thermodynamic quantities as well as probability distributions were considered. The integration algorithm for the DPD-E variant was further verified by considering equilibrium and nonequilibrium simulation scenarios. Finally, we discussed the inevitable small, long-term drift in E associated with finite integration methods, where we proposed a simple strategy to minimize the effect of this drift in DPD-E simulations.

Implementing the SSA for a given conservative force potential, we found that a smaller time step is required for a DPD-E simulation, relative to the time step of a constant-temperature DPD simulation. This behavior is consistent with the analogs of MD integration algorithms. Moreover, the relative sizes of the time steps of constant-temperature DPD versus DPD-E simulations are comparable to the relative sizes of the time steps for canonical versus microcanonical MD simulations. Finally, and perhaps most importantly, compared to standard DPD integrators (17), while the SSA allows for modest increases in the size of the time step for constant-temperature DPD simulations, the SSA allows for much larger time steps for DPD-E simulations. Comparing with the recent study of Abu-Nada that used the standard velocity-Verlet algorithm for DPD-E simulations of the DPD fluid model (18, 19), the SSA proposed in this work allows for time steps as much as 10^3 times larger, which is an essential improvement for practical applications of the DPD-E method. So while the computational cost of the SSA is almost twice that of the standard velocity-Verlet algorithm, this cost is compensated by allowing larger time steps.

6. References

1. Hoogerbrugge, P. J.; Koelman, J. M. V. A. Simulating Microscopic Hydrodynamic Phenomena With Dissipative Particle Dynamics. *Europhys. Lett.* **1992**, *19*, 155.
2. Koelman, J. M. V. A.; Hoogerbrugge, P. J. Dynamic Simulation of Hard Sphere Suspensions Under Steady Shear. *Europhys. Lett.* **1993**, *21*, 363.
3. Bonet Avalos, J.; Mackie, A. D. Dissipative Particle Dynamics With Energy Conservation. *Europhys. Lett.* **1997**, *40*, 141.
4. Español, P. Dissipative Particle Dynamics With Energy Conservation. *Europhys. Lett.* **1997**, *40*, 631.
5. Nikunen, P.; Karttunen, M.; Vattulainen, I. How Would You Integrate the Equations of Motion in Dissipative Particle Dynamics Simulations? *Comp. Phys. Comm.* **2003**, *153*, 407.
6. Groot, R. D.; Warren, P. B. Dissipative Particle Dynamics: Bridging the Gap Between Atomistic and Mesoscopic Simulation. *J. Chem. Phys.* **1997**, *107*, 4423.
7. Abu-Nada, E. Natural Convection Heat Transfer Simulation Using Energy Conservative Dissipative Particle Dynamics. *Phys. Rev. E* **2010**, *81*, 056704.
8. Abu-Nada, E. Application of Dissipative Particle Dynamics to Natural Convection in Differentially Heated Enclosures. *Molecular Simulation* **2011**, *37*, 135.
9. Chaudhri, A.; Lukes, J. R. Velocity and Stress Autocorrelation Decay in Isothermal Dissipative Particle Dynamics. *Phys. Rev. E* **2010**, *81*, 026707.
10. Shardlow, T. Splitting for Dissipative Particle Dynamics. *SIAM J. Sci. Comput.* **2003**, *24*, 1267.
11. Brennan, J. K.; Lísal, M. *Dissipative Particle Dynamics at Isothermal Conditions Using Shardlow-Like Splitting Algorithms*; ARL-TR-6582; U.S. Army Research Laboratory: Aberdeen Proving Ground, MD, September 2013.
12. Brennan, J. K.; Lísal, M. *Dissipative Particle Dynamics at Isothermal, Isobaric Conditions Using Shardlow-Like Splitting Algorithms*; ARL-TR-6583; U.S. Army Research Laboratory: Aberdeen Proving Ground, MD, September 2013.
13. Brennan, J. K.; Lísal, M. *Proceedings of the 14th International Detonation Symposium*, Coeur d'Alene, ID, 11–16 April 2010; Office of Naval Research, 2010; pp 1451.
14. Pagonabarraga, I.; Frenkel, D. Dissipative Particle Dynamics for Interacting Systems. *J. Chem. Phys.* **2001**, *115*, 5015.

15. Merabia, S.; Bonet Avalos, J. Dewetting of a Stratified Two-Component Liquid Film on a Solid Substrate. *J. Phys. Rev. Lett.* **2008**, *101*, 208303.
16. Mackie, A. D.; Bonet Avalos, J.; Navas, V. Dissipative Particle Dynamics With Energy Conservation: Modelling of Heat Flow. *Phys. Chem. Chem. Phys.* **1999**, *1*, 2039.
17. Stoltz, G. A Reduced Model for Shock and Detonation Waves. I. The Inert Case. *Europhys. Lett.* **2006**, *76*, 849.
18. Ripoll, M.; Ernst, M. H. Model System for Classical Fluids out of Equilibrium. *Phys. Rev. E* **2004**, *71*, 041104.
19. McQuarrie, D. A. *Statistical Mechanics*; University Science Books: Sausalito, CA 2000.
20. Ripoll, M.; Español, P.; Ernst, M. H. Dissipative Particle Dynamics With Energy Conservation: Heat Conduction. *Int. J. Mod. Phys. C* **1998**, *9*, 1329.
21. Allen, M. P.; Tildesley, D. J. *Computer Simulation of Liquids*; Clarendon Press: Oxford, UK, 1987.
22. Frenkel, D.; Smit, B. *Understanding Molecular Simulation: From Algorithms to Applications*; Academic Press: London, 2002.
23. Tuckerman, M. E.; Berne, B. J.; Martyna, G. J. Reversible Multiple Time Scale Molecular Dynamics. *J. Chem. Phys.* **1992**, *97*, 1990.
24. Hairer, E.; Lubich, C.; Wanner, G. Geometric Numerical Integration. *Structure-Preserving Algorithms for Ordinary Differential Equations*; Springer Verlag: Berlin, 2006.
25. Leimkuhler, B.; Reich, S. *Simulating Hamiltonian Dynamics*; Cambridge University Press: Cambridge, UK, 2004.

Appendix A. Fokker-Planck Equation and Fluctuation-Dissipation Theorem

Here, we summarize the Fokker-Planck equation (FPE) and outline the derivation of the fluctuation-dissipation theorem (FDT) for the dissipative particle dynamics method at constant energy (DPD-E) variant considered in the report. The FPE corresponding to the equations of motion (EOMs) given by equation 5 of the report is

$$\frac{\partial \rho}{\partial t} = L_C \rho + L_D \rho + L_{cond} \rho, \quad (\text{A-1})$$

where the conservative operator L_C is given by

$$L_C \equiv - \left(\sum_i \frac{\mathbf{p}_i}{m_i} \cdot \frac{\partial}{\partial \mathbf{r}_i} + \sum_i \sum_{j \neq i} \mathbf{F}_{ij}^C \cdot \frac{\partial}{\partial \mathbf{p}_i} \right). \quad (\text{A-2})$$

The operator representing the effects of the dissipative and random forces is given by

$$L_D \equiv \sum_i \sum_{j \neq i} \frac{\mathbf{r}_{ij}}{r_{ij}} \cdot \left(\frac{\partial}{\partial \mathbf{p}_i} - \frac{\mathbf{v}_{ij}}{2} \frac{\partial}{\partial u_i} \right) \left[\gamma_{ij} \omega^D \left(\frac{\mathbf{r}_{ij}}{r_{ij}} \cdot \mathbf{v}_{ij} \right) + \frac{\sigma_{ij}^2}{2} (\omega^R)^2 L_{ij} \right], \quad (\text{A-3})$$

$$L_{ij} = \frac{\mathbf{r}_{ij}}{r_{ij}} \cdot \left[\frac{\partial}{\partial \mathbf{p}_i} - \frac{\partial}{\partial \mathbf{p}_j} - \frac{\mathbf{v}_{ij}}{2} \left(\frac{\partial}{\partial u_i} + \frac{\partial}{\partial u_j} \right) \right]$$

while the operator associated with the effects of the mesoscopic heat transfer between particles is given by

$$L_{cond} \equiv - \left\{ \sum_i \sum_{j \neq i} \omega^{Dq} \frac{\partial}{\partial u_i} \left[\kappa_{ij} \left(\frac{1}{\theta_i} - \frac{1}{\theta_j} \right) \right] - \frac{1}{2} (\omega^{Rq})^2 \frac{\partial}{\partial u_i} \left[\alpha_{ij}^2 \left(\frac{\partial}{\partial u_i} - \frac{\partial}{\partial u_j} \right) \right] \right\} \quad (\text{A-4})$$

with the condition $\left(\frac{\partial}{\partial u_i} - \frac{\partial}{\partial u_j} \right) \alpha_{ij}^2 = 0$ to ensure that the EOMs contain no spurious drift.

In equations A-1 through A-4, $\rho \equiv \rho(\mathbf{r}, \mathbf{p}, u; t)$ and $u \equiv \{u_i\}_{i=1}^N$ are the particle internal energies; κ_{ij} and α_{ij} are the mesoscopic thermal conductivity and noise amplitude between particle i and particle j , respectively; ω^{Dq} and ω^{Rq} are weight functions associated with the mesoscopic heat transfer between particles; and $\theta_i \equiv \frac{\partial u_i}{\partial s_i}$ is the internal temperature (s_i is the mesoscopic entropy of particle i).

In contrast to constant-temperature DPD, an implicit heat reservoir is not present in constant-energy DPD. Furthermore, the FPE (A-1) does not impose external constraints on the system (such as the total system energy). Thus, for the purposes of deriving the FDT, it is equivalent to consider that the system is either isolated or in thermal contact with a heat reservoir, while the resulting FDT relations for either choice should be insensitive to any external constraints. The

use of the canonical distribution simplifies this derivation. Therefore, if we consider that the system is in contact with a heat reservoir that maintains the system temperature T , then $\rho^{eq} \equiv \rho^{eq}(\mathbf{r}, \mathbf{p}, u)$ corresponds to the canonical probability density

$$\rho^{eq}(\mathbf{r}, \mathbf{p}, u) = \frac{1}{Z} \exp \left(- \frac{\sum_i \frac{\mathbf{p}_i \cdot \mathbf{p}_i}{2m_i} + \sum_i \sum_{j>i} u_{ij}^{CG}}{k_B T} \right) \prod_i \exp \left[\frac{s_i(u_i)}{k_B} - \frac{u_i}{k_B T} \right]. \quad (\text{A-5})$$

Similarly as before, $L_C \rho^{eq} = 0$,¹ while the FDT then follows from the requirements that $L_D \rho^{eq} = 0$ and $L_{cond} \rho^{eq} = 0$. $L_D \rho^{eq} = 0$ is satisfied for

$$\sigma_{ij}^2 (\omega^R)^2 = 2\gamma_{ij} \omega^D k_B \Theta_{ij},$$

i.e., for

$$\begin{aligned} \sigma_{ij}^2 &= 2\gamma_{ij} k_B \Theta_{ij} \\ (\omega^R)^2 &= \omega^D \end{aligned}, \quad (\text{A-6})$$

where $\Theta_{ij}^{-1} = \frac{1}{2} \left(\frac{1}{\theta_i} + \frac{1}{\theta_j} \right)$, while $L_{cond} \rho^{eq} = 0$ is satisfied for

$$\alpha_{ij}^2 (\omega^{Rq})^2 = 2k_B \kappa_{ij} \omega^{Dq},$$

i.e., for

$$\begin{aligned} \alpha_{ij}^2 &= 2k_B \kappa_{ij} \\ (\omega^{Rq})^2 &= \omega^{Dq} \end{aligned}. \quad (\text{A-7})$$

Generally, κ_{ij} can be a function of u_i and u_j . For such a case, $L_{cond} \rho^{eq} = 0$ requires that $\kappa_{ij} = \kappa(u_i + u_j)$ because of the constraint on α_{ij}^2 given in equation A-4. As expected, the FDT relations, equations A-6 and A-7, do not depend on the heat reservoir temperature and therefore do not depend on the ensemble used for the derivation of these relations.

¹Brennan, J. K.; Lísal, M. *Dissipative Particle Dynamics at Isothermal Conditions Using Shardlow-Like Splitting Algorithms*; ARL-TR-6582; U.S. Army Research Laboratory: Aberdeen Proving Ground, MD, September 2013.

INTENTIONALLY LEFT BLANK.

Appendix B. Simulation Model Details

For the models considered in this work, the details of the conservative forces expressed in equation 2 of the main text are the following. u_{ij}^{CG} for the pure and binary Dissipative Particle Dynamics (DPD) fluid models is given by

$$u_{ij}^{CG} = a_{ij} r_c \omega^D(r_{ij}), \quad (\text{B-1})$$

where a_{ij} is the maximum repulsion between particle i and particle j .

For the coarse-grain solid model, which has a face-centered-cubic (f.c.c.) lattice structure, particles interact through a shifted-force Sutton-Chen embedded potential (SC) embedded potential given as:

$$u_i^{CG} = \varepsilon \left(\frac{1}{2} \sum_{j \neq i} u_{ij}^{rep} - c \sqrt{\rho_i} \right), \quad (\text{B-2})$$

where

$$\begin{aligned} u_{ij}^{rep} &= v(r_{ij}) - v(r_{ij} = r_c) - \left. \frac{dv(r_{ij})}{dr_{ij}} \right|_{r_{ij}=r_c} (r_{ij} - r_c) \\ v(r_{ij}) &= \left(\frac{r_0}{r_{ij}} \right)^n \\ \rho_i &= \sum_{j \neq i} \rho_{ij} \\ \rho_{ij} &= w(r_{ij}) - w(r_{ij} = r_c) - \left. \frac{dw(r_{ij})}{dr_{ij}} \right|_{r_{ij}=r_c} (r_{ij} - r_c) \\ w(r_{ij}) &= \left(\frac{r_0}{r_{ij}} \right)^m \end{aligned} \quad (\text{B-3})$$

ε and r_0 are the energy and length parameters, respectively, n and m are positive integers ($n > m$ to satisfy elastic stability of the crystal), and c is a dimensionless parameter. Although effectively this is a many-body potential, the force on each particle can be written as a sum of pairwise contributions. The coarse-grain solid model used here approximates nickel, where one DPD particle was chosen to represent four f.c.c. unit cells, i.e., 16 nickel (Ni) atoms. SC potential parameters were determined by fitting to various 0-K properties and the melting temperature at zero pressure,¹ where the following values were found: $\varepsilon/k_B = 225$ K, $r_0 = 8.8698$ Å, $c = 39.4314$, $m = 6$, and $n = 9$. Further details for determining SC parameters based upon such a procedure can be found elsewhere.^{2,3}

¹WebElements. <http://www.webelements.com/> (accessed 16 August 2013).

²Brennan, J. K.; Lísal, M. *Proceedings of the 14th International Detonation Symposium*, Coeur d'Alene, ID, 11–16 April 2010.

³Sutton, A. P.; Chen, J. Long-Range Finnis Sinclair Potentials. *J. Philos. Mag. Lett.* **1990**, *61*, 139.

List of Symbols, Abbreviations, and Acronyms

DPD	constant-temperature Dissipative Particle Dynamics
DPD-E	constant-energy Dissipative Particle Dynamics
EOMs	equations of motion
f.c.c.	face-centered-cubic
FDT	fluctuation-dissipation theorem
FPE	Fokker-Planck equation
MD	molecular dynamics
SC	Sutton-Chen embedded potential
SDEs	stochastic differential equations
SSA	Shardlow-splitting algorithm
SSA-VV	Shardlow-splitting algorithm-velocity Verlet

NO. OF
COPIES ORGANIZATION

1 DEFENSE TECHNICAL
(PDF) INFORMATION CTR
DTIC OCA

1 DIRECTOR
(PDF) US ARMY RESEARCH LAB
IMAL HRA

1 DIRECTOR
(PDF) US ARMY RESEARCH LAB
RDRL CIO LL

1 GOVT PRINTG OFC
(PDF) A MALHOTRA

ABERDEEN PROVING GROUND

1 DIR USARL
(PDF) RDRL WML B
J BRENNAN